

# Securing MIMO Wiretap Channel with Learning-Based Friendly Jamming under Imperfect CSI

Bui Minh Tuan, Diep N. Nguyen, Nguyen Linh Trung, Van-Dinh Nguyen, Nguyen Van Huynh, Dinh Thai Hoang, Marwan Krunz, and Eryk Dutkiewicz

**Abstract**—Wireless communications are particularly vulnerable to eavesdropping attacks due to their broadcast nature. To effectively deal with eavesdroppers, existing security techniques usually require accurate channel state information (CSI), e.g. for friendly jamming (FJ), and/or additional computing resources at transceivers, e.g. cryptography-based solutions, which unfortunately may not be feasible in practice. This challenge is even more acute in low-end IoT devices. We thus introduce a novel deep learning-based FJ framework that can effectively defeat eavesdropping attacks with imperfect CSI and even without CSI of legitimate channels. In particular, we first develop an autoencoder-based communication architecture with FJ, namely AEFJ, to jointly maximize the secrecy rate and minimize the block error rate at the receiver without requiring perfect CSI of the legitimate channels. In addition, to deal with the case without CSI, we leverage the mutual information neural estimation (MINE) concept and design a MINE-based FJ scheme that can achieve comparable security performance to the conventional FJ methods that require perfect CSI. Extensive simulations in a multiple-input multiple-output (MIMO) system demonstrate that our proposed solution can effectively deal with eavesdropping attacks in various settings. Moreover, the proposed framework can seamlessly integrate MIMO security and detection tasks into a unified end-to-end learning process. This integrated approach can significantly maximize the throughput and minimize the block error rate, offering a good solution for enhancing communication security in wireless communication systems.

**Index Terms**—Autoencoder, IoT security, anti-eavesdropping, friendly jamming, multiple-input-multiple-output (MIMO), mutual information, physical layer security, wiretap channel, mutual information neural estimation (MINE).

## I. INTRODUCTION

The rapid development of the Internet of Things (IoT) has paved the way for establishing connections and gathering data across various domains, from smart homes and cities, to healthcare, transportation, and Industry 4.0. However, with

a large number of diverse wireless devices, IoT networks are highly vulnerable to adversaries due to the broadcast nature of wireless communications. Among radio threats, eavesdropping is one of the most common and dangerous attacks. Specifically, with off-the-shelf circuits, adversaries can effectively launch eavesdropping attacks to passively wiretap legitimate wireless channels to intercept the transmitted information from the transmitter. As a result, the need for lightweight anti-eavesdropping approaches that accommodate the limited processing capabilities of IoT devices without compromising their operational efficiency is, therefore, critical.

### A. Related Work

The most common countermeasure against eavesdroppers is encryption techniques [1], such as Advanced Encryption Standard (AES) and Rivest-Shamir-Adelman (RSA). Unfortunately, these methods require infrastructure for distributing public keys and the irresistibility of the underlying encrypted function. In addition, data encryption and decryption create burdens on computing resources for wireless devices, especially for computing- and resource-constrained devices such as IoT devices and wireless sensors [2], [3]. Moreover, conventional encryption techniques may not guarantee absolute protection when eavesdroppers have sufficient computational capability or employ sophisticated techniques to crack encryption keys [1]. Hence, when transceivers have limited capabilities as compared to eavesdroppers, such as IoT devices, legitimate communication links are still subject to being compromised. Finally, quantum computing may soon crack encryption techniques while post-quantum cryptography is still in its infancy and may not be feasible/suitable for power-constrained devices [4].

Given the limitations of encryption techniques, physical layer security (PLS) has emerged as a promising solution to deal with eavesdropping attacks by leveraging the dynamic and stochastic nature of wireless channels [5]. Specifically, PLS aims to achieve a positive secrecy capacity defined by the difference between the channel capacities of the legitimate link and the eavesdropper link [6], [7]. To do that, PLS can focus on either random key generation or provisioning information-theoretic secrecy rates to design secure wireless communication systems [8]. The former extracts channel state information (CSI) to generate random keys that can be used for authentication purposes. The latter includes channel coding,

Bui Minh Tuan, Diep N. Nguyen, Dinh Thai Hoang, and Eryk Dutkiewicz are with the School of Electrical and Data Engineering, University of Technology Sydney, NSW 2007, Australia (bui.m.tuan@student.uts.edu.au; {diep.nguyen, hoang.dinh, eryk.dutkiewicz} @uts.edu.au).

Van-Dinh Nguyen is with the College of Engineering and Computer Science and the Center for Environmental Intelligence, VinUniversity, Vinhomes Ocean Park, Hanoi, Vietnam (dinh.nv2@vinuni.edu.vn).

Nguyen Van Huynh is with the School of Computing, Engineering and the Built Environment, Edinburgh Napier University, Edinburgh EH10 5DT, UK. (h.nguyen2@napier.ac.uk).

Marwan Krunz is with the Department of Electrical and Computer Engineering, The University of Arizona, Tucson, AZ, USA (krunz@arizona.edu).

Nguyen Linh Trung (correspondence) is with the Advanced Institute of Engineering and Technology, University of Engineering and Technology, Vietnam National University, Hanoi, Vietnam (linhtrung@vnu.edu.vn).

channel-based adaptation, and artificial noise (AN)/friendly jamming (FJ)-based security. Among these PLS approaches, the FJ technique has been widely studied in the literature due to its effectiveness in dealing with eavesdropping attacks. With the FJ technique, the transmitter (Tx) uses a proportion of the transmit power to deliberately inject noise signals to degrade the reception of the legitimate signals at eavesdroppers while not adversely impacting the legitimate receiver (Rx) [7]. This can be achieved with the beamforming technique that is popular in multi-input, multi-output or multi-input-multi-output (MIMO) systems. The critical factor affecting the security performance of FJ is the availability of CSI at the Tx for beamforming purposes. In one of the early studies on FJ-based security [9], Tx-based friendly jamming (TxFJ) and cooperative jamming were proposed with the assumption that the perfect CSI between legitimate transceivers is known at the Tx. The FJ signal is then designed to project on the nullspace/directions of the legitimate channel so that the FJ noise signal will not affect the signal-to-noise ratio (SNR) of the Rx. Rx-based friendly jamming (RxFJ) was also proposed with a multi-user broadcast channel in [10], guaranteeing a non-zero average secrecy rate, regardless of the position of the eavesdropper.

Securing multi-user link while managing the adverse effect of the FJ interference was further studied in [11]. The authors used a non-cooperative game to model the FJ and transmit power control problem for the interfering wiretap links. In addition, the work in [12] investigated beamforming based-FJ to achieve an instantaneous secrecy rate. In particular, the authors first derived the closed-form secrecy rate. Then, the Tx picks a suitable coding scheme to guarantee secrecy. Nevertheless, all the above methods as well as most general MIMO settings e.g., [9]–[11], [13]–[15] required or assumed perfect CSI or, at least, statistical CSI of the legitimate channel at the Tx to construct FJ signals. However, perfect or statistical CSI acquisition is very challenging, if not impractical, especially for IoT communications.

The key reasons are the inaccuracy of the estimated CSI at the Rx (before feeding it back to the Tx) and the limited bandwidth of the feedback channel [16]. Hence, the FJ signals, designed to lie on the nullspace of the imperfect channel [9], [10], may degrade the quality of the (actual) legitimate channel and not be fully canceled out at the Rx. To overcome these issues, the authors in [12], [17], [18] assumed statistical CSI (instead of full/complete CSI) to satisfy the QoS of SNR and the nonzero secrecy capacity. Then, the second perturbation analysis was used to design the beamforming scheme. Unfortunately, this method requires high computational capability at the Rx and high running time. Another approach in [18] proposed a masked beamforming scheme that leverages artificial noise to impair the decoding capabilities the eavesdropper, particularly regarding channel estimation delay and error. The instantaneous security performance of this scheme was then evaluated in terms of the minimum mean square error at the eavesdropper, providing a metric to assess its effectiveness in enhancing communication security amidst the discussed challenges. However, the alternative optimization used in the proposed approach has a low convergence

speed. Furthermore, the work in [19] introduced an FJ-based authentication scheme. This scheme leverages FJ to obscure a hash-based message authentication code tag, facilitating secure authentication between legitimate users. Although achieving good security performance, this method may add significant overhead to the current communication infrastructure.

## B. Motivation and Main Contributions

As mentioned earlier, the security performance of FJ-based methods is highly affected by imperfect CSI (ImCSI). To cope with it, conventional methods were based on exhaustive search and second-order statistics that require high computational and transmission overhead. This work aims to develop an FJ solution based on deep learning (DL) in order to deal with ImCSI. To this end, we integrate the autoencoder (AE) architecture, with denoising and generalization capability, into the FJ approach. AE is designed to acquire a dataset representation (encoding) and reconstruct (decoding) the input from the output. Based on this encoding, it reconstructs a representation of the output that closely resembles the input [20], [21]. Unlike the previous works in [17], [22]–[24], and [25], we introduce a novel FJ method for PLS utilizing AE while the statistical information of channel estimation error is known. Consequently, the running time and overhead of our DL-based method can be reduced significantly compared to the conventional methods.

Moreover, to deal with the case without even statistical CSI (SCSI) at the transmitter, we integrate the method of mutual information neural estimation (MINE) [23] into our AE architecture. MINE has been employed for transceiver design in a few studies in the literature. For example, the authors in [26] adopted MINE to improve the channel coding process at the transmitter. Differently, the authors in [24] demonstrated that combining AE and MINE could enhance transmission performance, including decoding error and throughput. However, these works and others in the literature only considered single-input-single-output systems and may not be effective when dealing with eavesdropping attacks. Our study here expands upon the traditional concept of relying on perfect CSI to cancel out FJ at the Rx. In particular, our method empowers the legitimate Tx and Rx to learn how to suppress FJ signals while maintaining the degradation of the eavesdropper channel.

Our work has three main contributions. Firstly, we propose a novel joint optimization framework that maximizes the secrecy rate while minimizing the block/symbol error rates, based on end-to-end (E2E) learning with a new loss security function. This novel framework enables us to explore the interplay between MIMO secrecy optimization and detection.

Secondly, we use generalization capabilities inherent in deep neural networks to develop an AE-based FJ scheme that exhibits robustness against challenges posed by SCSI. These challenges arise due to various factors such as dynamic channel variations or constraints imposed by a limited number of pilots as studied in [27]. Given the strong capability of DL-based communication frameworks to handle diverse input datasets, our method showcases a superior secrecy rate as compared to conventional methods, especially when dealing

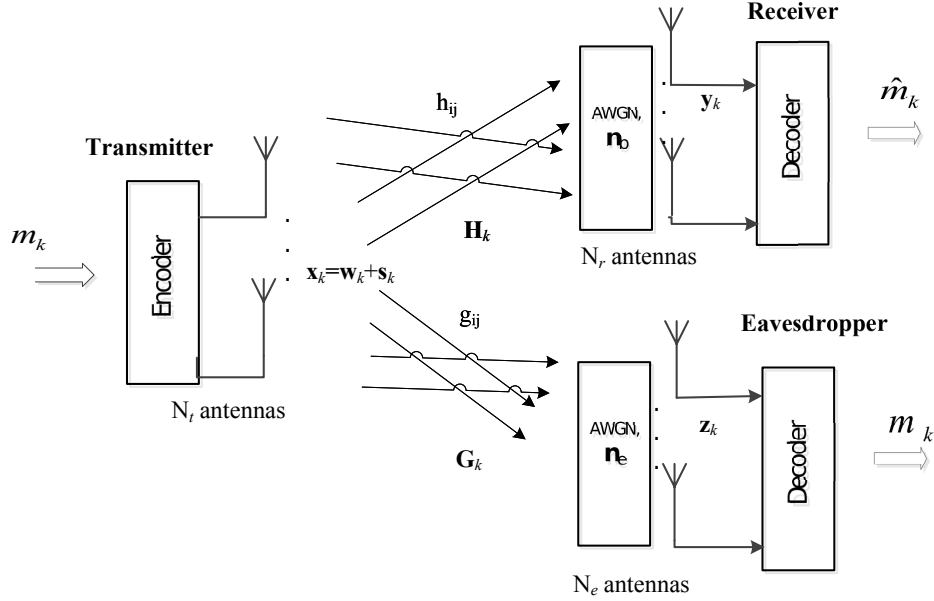


Fig. 1: Illustration of MIMO FJ-based system model with Tx, Rx, and eavesdropper.

with channel estimation errors. To achieve this, the secrecy rate optimization is integrated into the E2E learning process under SCS scenarios.

Thirdly, for the case without SCS, we leverage the MINE-based FJ to show that attaining a level of security equivalent to traditional FJ methods with perfect CSI is feasible. During training, the mutual information (MI) of the legitimate channel is maximized while that of the eavesdropper is minimized using the inputs as the samples taken from Tx and Rx signals. Different from the E2E AE-based FJ in the second contribution, the MINE-based FJ minimizes the computational burden and conserves energy consumption at the Rx. This methodology is particularly suitable for applications in IoT networks where devices have limited computational resources.

Extensive simulations/experiments are carried out to demonstrate the effectiveness of the proposed method AEFJ in terms of secrecy throughput and block error rate.

The structure of this paper is as follows: Section II provides a brief overview of the system model and the FJ-based Physical Layer Security (PLS) technique as a reference point for our new approach. Following this, Section III details our novel AE-based FJ strategy, designed to counter eavesdroppers when only statistical information of channel estimation error is available. Section IV-B introduces our security framework utilizing MINE to safeguard communications without CSI. The analysis of secrecy and Block Error Rate (BLER) by simulations is presented in Section V. Conclusions are drawn in Section VI.

**Notation:** Vectors and matrices are denoted by bold lowercase and uppercase letters, respectively. The absolute value of a real number, the magnitude of a complex number, and the complex conjugate transpose are, respectively, denoted by  $\|\cdot\|$ ,  $|\cdot|$  and  $(\cdot)^\dagger$ . The complex Gaussian random variable with mean  $\mu$  and variance  $\sigma^2$  is denoted by  $CN(\mu, \sigma^2)$ .  $\mathbb{E}[X]$  denotes the expectation of  $X$ ,  $\text{Tr}(\mathbf{A})$  the trace of the square matrix  $\mathbf{A}$ .

## II. SYSTEM MODEL AND SECRECY RATE OPTIMIZATION

### A. Background on MIMO-FJ

1) *System Model:* The standard MIMO FJ model is depicted in Fig. 1, where the Tx, the Rx, and the eavesdropper are equipped with  $N_t$ ,  $N_r$  and  $N_e$  antennas, respectively [9]. Channel matrices at time slot  $k$  for the Tx-Rx and Tx-eavesdropper links are denoted as  $\mathbf{H}_k \in \mathbb{C}^{N_r \times N_t}$  and  $\mathbf{G}_k \in \mathbb{C}^{N_e \times N_t}$ . Each element of  $\mathbf{H}_k$  and  $\mathbf{G}_k$  is assumed to be known, i.i.d., and unchanged over a block of transmit symbols. Let  $\mathbf{s}_k$  be the desired message to the Rx. To cancel interference caused by FJ at the Rx, the FJ signal  $\mathbf{w}_k$  is designed to satisfy  $\mathbf{H}_k^\dagger \mathbf{w}_k = 0$ . Given the transmitted signal  $\mathbf{x}_k = \mathbf{s}_k + \mathbf{w}_k$ , the received signals at the Rx and the eavesdropper can be expressed as follows:

$$\mathbf{y}_k = \mathbf{H}_k^\dagger \mathbf{x}_k + \mathbf{n}_b = \mathbf{H}_k^\dagger \mathbf{s}_k + \mathbf{H}_k^\dagger \mathbf{w}_k + \mathbf{n}_b, \quad (1)$$

$$\mathbf{z}_k = \mathbf{G}_k^\dagger \mathbf{s}_k + \mathbf{G}_k^\dagger \mathbf{w}_k + \mathbf{n}_e \quad (2)$$

where  $\mathbf{n}_b \sim CN(0, \sigma_b^2)$  and  $\mathbf{n}_e \sim CN(0, \sigma_e^2)$  are the additive white Gaussian noise (AWGN) at the Rx and the eavesdropper. The FJ signal  $\mathbf{w}_k$  is designed as  $\mathbf{w}_k = \mathbf{Z}_k \mathbf{v}_k$ , where the precoding matrix  $\mathbf{Z}_k$  is the orthogonal basis of the nullspace of  $\mathbf{H}_k^\dagger$ . The elements of  $\mathbf{v}_k$  are i.i.d. complex Gaussian random variables with variance  $\sigma_v^2$ . The noise covariance at the eavesdropper then can be calculated as follows:

$$\mathbf{K}_k = (\mathbf{G}_k^\dagger \mathbf{Z}_k^\dagger \mathbf{Z}_k \mathbf{G}_k) \sigma_v^2 + \mathbf{I}_{N_e} \sigma_e^2, \quad (3)$$

where  $\mathbf{I}_i$  is an  $i \times i$  identity matrix.

2) *The Secrecy Rate Optimization Problem:* Given  $R_{AB}$  and  $R_{AE}$  as the legitimate and illegitimate channel rates, the secrecy rate  $R_k^s$  (nats/s/Hz) is given by

$$\begin{aligned} R_k^s &\triangleq [R_{AB} - R_{AE}]_+ = [\log(1 + \text{SINR}_B) - \log(1 + \text{SINR}_E)]_+ \\ &= \left[ \log \det(\mathbf{I} + \mathbf{H}_k^\dagger \mathbf{Q}_s \mathbf{H}_k) - \log \frac{\det(\mathbf{K}_k + \mathbf{G}_k^\dagger \mathbf{Q}_s \mathbf{G}_k)}{\det(\mathbf{K}_k)} \right]_+ \end{aligned} \quad (4)$$

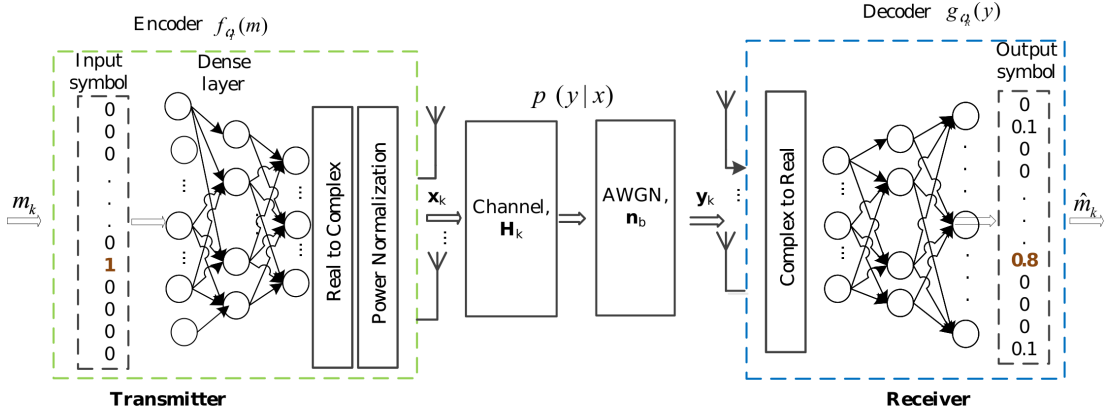


Fig. 2: The AE-based communication with E2E learning.

where  $[x]_+ = \max(0, x)$ ,  $\mathbf{Q}_s = \mathbf{E}[\mathbf{s}_k \mathbf{s}_k^\dagger]$ . Since the eavesdropper's CSI is unavailable at the Tx, we focus on maximizing the first term in (4) by using singular value decomposition (SVD). Specifically, the legitimate channel  $\mathbf{H}_k$  is first decomposed as

$$\mathbf{H}_k^\dagger = \mathbf{U}_k \mathbf{\Gamma}_k \mathbf{V}_k^\dagger, \quad (5)$$

where  $\mathbf{U}_k \in \mathbb{C}^{N_r \times N_r}$ ,  $\mathbf{V}_k \in \mathbb{C}^{N_t \times N_t}$ , and  $\mathbf{\Gamma}_k \in \mathbb{C}^{N_t \times N_t}$ . After precoding  $\mathbf{r}_k = \mathbf{V}_k^\dagger \mathbf{s}_k$ , the received signal  $\mathbf{y}_k$  is multiplied with  $\mathbf{U}_k^\dagger$ . Then, the received signal in (1) can be equivalently to

$$\tilde{\mathbf{y}}_k = \mathbf{\Gamma}_k^\dagger \mathbf{r}_k + \tilde{\mathbf{n}}_b, \quad (6)$$

where  $\tilde{\mathbf{y}}_k = \mathbf{U}_k^\dagger \mathbf{y}_k$ . We denote  $P$  is the total transmit power,  $P_{\text{info}}$  is the power for transmitting information signal, and  $\mathbf{Q}_r$  as the precoded transmit covariance. Then  $\mathbf{Q}_r$  is designed as

$$\mathbf{Q}_r = \mathbb{E}[\mathbf{r}_k \mathbf{r}_k^\dagger] = \text{diag}(\sigma_{r,1}^2, \sigma_{r,2}^2, \dots, \sigma_{r,N_t}^2), \quad (7)$$

where  $\sigma_{r,i}^2$  is derived by the water filling solution with power constraint  $P_{\text{info}} \leq P$ , corresponding to the  $N_t$  largest singular values of  $\mathbf{H}_k^\dagger$ . Thus, the secrecy rate  $R_k^s$  is re-expressed as

$$R_k^s = \left[ \log \det(\mathbf{I} + \mathbf{\Gamma}_k \mathbf{Q}_r \mathbf{\Gamma}_k^\dagger) - \log \frac{\det(\mathbf{K}_k + \mathbf{F}_k)}{\det(\mathbf{K}_k)} \right]_+, \quad (8)$$

where  $\mathbf{F}_k = \mathbf{G}_k^\dagger \mathbf{V}_k^\dagger \mathbf{Q}_r \mathbf{V}_k \mathbf{G}_k$ . Since  $R_k^s$  is random, the average secrecy rate over a number of channel realizations  $\bar{R}$  will be used. Our objective is to maximize the average secrecy rate subject to the power constraint at the Tx, which is mathematically formulated as follows:

$$\bar{R} \doteq \max_{\text{Tr}(\mathbb{E}[\mathbf{x}_k \mathbf{x}_k^\dagger]) \leq P} \mathbb{E} \left[ \log \det(\mathbf{I} + \mathbf{\Gamma}_k \mathbf{Q}_r \mathbf{\Gamma}_k^\dagger) - \log \frac{\det(\mathbf{K}_k + \mathbf{F}_k)}{\det(\mathbf{K}_k)} \right]. \quad (9)$$

The power constraint  $\text{Tr}(\mathbb{E}[\mathbf{x}_k \mathbf{x}_k^\dagger]) \leq P$  can be rewritten as  $\text{Tr}(\mathbf{V}_k^\dagger \mathbf{Q}_r \mathbf{V}_k + N_{\text{FJ}} \sigma_v^2 \mathbf{I}_{N_t}) \leq P$ , where  $N_{\text{FJ}}$  denotes the number of dimensions used for transmitting FJ signals.

3) *Channel Estimation Error Model*: The previous part considers the case of perfect CSI. Regarding ImCSI, due to channel estimation error, we choose a common ImCSI model [17]:

$$\tilde{\mathbf{H}}_k = \mathbf{H}_k + \Delta \mathbf{H}_k, \quad (10)$$

where the channel estimation error  $\Delta \mathbf{H}_k$  is modeled as an i.i.d. complex Gaussian and circularly symmetric random matrix with the covariance  $\mathbf{C}_{\Delta \mathbf{H}_k} \sim \mathcal{CN}(\mathbf{0}, \rho_c^2 \mathbf{I}_{N_r})$ . Then the secrecy rate in (4) becomes

$$\bar{R}_k^s \doteq \max_{\text{Tr}(\mathbb{E}[\mathbf{x}_k^\dagger \mathbf{x}_k]) \leq P} \mathbb{E} \left[ \log \frac{\det(\mathbf{I} + (\mathbf{H}_k + \Delta \mathbf{H}_k)^\dagger \mathbf{Q}_s (\mathbf{H}_k + \Delta \mathbf{H}_k))}{\det(\mathbf{D}_k)} - \log \frac{\det(\mathbf{K}_k + \mathbf{G}_k^\dagger \mathbf{Q}_s \mathbf{G}_k)}{\det(\mathbf{K}_k)} \right], \quad (11)$$

where  $\mathbf{D}_k = (\Delta \mathbf{H}_k^\dagger \mathbf{Z}_k^\dagger \mathbf{Z}_k \Delta \mathbf{H}_k) \sigma_v^2 + \mathbf{I}_{N_r} \sigma_b^2$  is the noise covariance at the receiver. The reason is the FJ signals are not completely canceled out at the receiver due to channel error.

### B. AE-based MIMO Communication

The AE-based communication is illustrated in Fig. 2 [28]. The model aims to reconstruct the input messages at time  $k$ ,  $m_k \in \mathcal{M} = \{1, 2, \dots, M\}$ , by minimizing the reconstruction error of the inputs or transmitted signals. The message  $m_k$  is generated uniformly and then embedded into the transmitted symbol  $\mathbf{s}_k$ . Then, it is sent through the dense layers to generate the transmit signal  $\mathbf{x}_k$ . The batch normalization layer performs the power constraint. The decoder includes the complex to real conversion layer, dense layers, and the last layer using the Softmax activation function. The output is the probability distribution  $\hat{\mathbf{m}}_k \in (0, 1)^{\text{card}(M)}$  over all messages (card denotes cardinality). Then, the maximum likelihood (ML) is used to estimate the transmitted signal and optimize the construction error by using the cross-entropy loss function [28], [29]. Hence, the decoded message  $\hat{m}_k$  will be the index of the element of  $\hat{\mathbf{m}}_k$  with the highest value.

**Re-parameterization**: Since DL models only work on real numbers, converting complex parameters to real values is necessary. As studied in [30], the complex parameters can be re-parameterized into new real parameters as follows:

$$\hat{\mathbf{x}}_k = \begin{bmatrix} \Re(\mathbf{x}_k) \\ \Im(\mathbf{x}_k) \end{bmatrix}, \quad \hat{\mathbf{y}}_k = \begin{bmatrix} \Re(\mathbf{y}_k) \\ \Im(\mathbf{y}_k) \end{bmatrix}, \\ \hat{\mathbf{n}}_b = \begin{bmatrix} \Re(\mathbf{n}_b) \\ \Im(\mathbf{n}_b) \end{bmatrix}, \quad \hat{\mathbf{H}}_k = \begin{bmatrix} \Re(\mathbf{H}_k) & -\Im(\mathbf{H}_k) \\ \Im(\mathbf{H}_k) & \Re(\mathbf{H}_k) \end{bmatrix}, \quad (12)$$

where  $\Re(\mathbf{z})$  and  $\Im(\mathbf{z})$  denote the real and imaginary parts of a complex number  $\mathbf{z}$ . We have  $\hat{\mathbf{x}}_k \in \mathbb{R}^{2N_t}$ ,  $\hat{\mathbf{y}}_k \in \mathbb{R}^{2N_r}$  and

$\hat{\mathbf{H}}_k \in \mathbb{R}^{2N_r \times 2N_t}$ . As a result, the received signal at the Rx in (1) can be equivalently written as follows:

$$\hat{\mathbf{y}}_k = \hat{\mathbf{H}}_k^\dagger \hat{\mathbf{x}}_k + \hat{\mathbf{n}}_b. \quad (13)$$

The transmitted signal is expressed as  $\hat{\mathbf{x}}_k = \hat{\mathbf{s}}_k + \hat{\mathbf{w}}_k$ , where  $\hat{\mathbf{w}}_k$  and  $\hat{\mathbf{s}}_k$  are the FJ and information-bearing signals, respectively. Then, the signals received at the Rx and the eavesdropper are given by

$$\hat{\mathbf{y}}_k = \hat{\mathbf{H}}_k^\dagger \mathbf{s}_k + \hat{\mathbf{H}}_k^\dagger \hat{\mathbf{w}}_k + \hat{\mathbf{n}}_b, \quad (14)$$

$$\hat{\mathbf{z}}_k = \hat{\mathbf{G}}_k^\dagger \mathbf{s}_k + \hat{\mathbf{G}}_k^\dagger \hat{\mathbf{w}}_k + \hat{\mathbf{n}}_e. \quad (15)$$

### III. AE-BASED FRIENDLY JAMMING

In this section, we leverage the AE-based communication model mentioned above (see Fig. 2) with ImCSI to design AE-based FJ. The E2E learning scheme aims to achieve two goals: maximizing the secrecy rate and minimizing the BLER at the Rx. The proposed AE-based MIMO FJ communication and security scheme is illustrated in Fig. 3. The FJ signal is generated via the FJ generator layer and is then injected into the transmitted signals  $\mathbf{x}_k$ . A straightforward approach to optimize the secrecy rate is to maximize the MI difference between the Tx and the Rx and design an FJ signal such that it degrades the eavesdropper channel. Next, we will detail this approach.

#### A. AE-based MI Optimization

It is worth noting that the communication and security tasks are transformed into the classification with the AE, Softmax activation function, and cross-entropy based security loss function [28]. The conventional work often assumes that the channel  $\mathbf{H}_k$  is perfectly known, based on which the average secrecy rate is achieved by maximizing the channel rate or  $I(A, B)$  of the legitimate channel and the precoded FJ signals  $\mathbf{w}_k$  are then designed to lie in the nullspace of  $\mathbf{H}_k$  so as to degrade the eavesdropper channel with the highest probability. Regarding ImCSI, the FJ signals may not completely lie in the true nullspace of  $\mathbf{H}_k$ . Thus, finding the optimal FJ signals that can be completely canceled out at the Rx and degrade the decoding capability of the eavesdropper is a nontrivial task; even the statistical information of channel estimation error is available at the Tx. Since AE-based communication can be seen as a classifier of transmitted messages and symbols, the MI between the input and the output on the legitimate channel,  $I(A, B)$ , can be maximized using Softmax and cross-entropy loss functions. The transmitted message and its label are denoted by the random variables  $\mathbf{m}$  and  $\mathbf{l}$ , respectively. The training data consists of  $M$  classes and  $N$  labeled instances denoted as  $\{(m_k, l_k)\}_{k=1}^N$ , where  $l_k \in \mathcal{M} = \{1, \dots, M\}$  is a class label of input  $m_k$ . For the task of reconstruction, let  $l_k$  be equal to  $m_k$ . The AE is now a neural classifier  $AE(\mathbf{m}, \mathbf{l})$  parameterized by  $\phi$ . It can be seen that  $\mathbf{m}$  and  $\mathbf{x}$  have the same probability distribution  $p(\mathbf{m})$ , similarly with  $p(\mathbf{l})$  and  $\mathbf{y}$ . Thus, the MI between  $\mathbf{x}$  and  $\mathbf{y}$  can be expressed as:

$$I(\mathbf{x}, \mathbf{y}) = I(\mathbf{m}, \mathbf{l}) = \sum_{m_k \in \mathcal{M}} \sum_{l_k \in \mathcal{M}} p(\mathbf{m}, \mathbf{l}) \log \frac{p(\mathbf{m}, \mathbf{l})}{p(\mathbf{m})p(\mathbf{l})}. \quad (16)$$

The MI  $I(\mathbf{m}, \mathbf{l})$  can be rewritten as follows:

$$I(\mathbf{m}, \mathbf{l}) = \mathbb{E}_{\mathbf{m}, \mathbf{l}} \log \frac{p(\mathbf{l}|\mathbf{m})}{p(\mathbf{l})}, \quad (17)$$

where  $\mathbb{E}_{\mathbf{m}, \mathbf{l}}$  is the expectation with respect to the joint distribution  $p(\mathbf{m}, \mathbf{l})$ . Since  $p(\mathbf{m}, \mathbf{l})$  is not available, we use the variational distribution  $q$  to estimate  $I(\mathbf{m}, \mathbf{l})$ . This can be done as follows [31]:

$$\begin{aligned} I(\mathbf{m}, \mathbf{l}) &= \mathbb{E}_{\mathbf{m}, \mathbf{l}} \log \frac{p(\mathbf{l}|\mathbf{m})}{p(\mathbf{l})} = \mathbb{E}_{\mathbf{m}, \mathbf{l}} \log \frac{q(\mathbf{l}|\mathbf{m})p(\mathbf{l}|\mathbf{m})}{p(\mathbf{l})q(\mathbf{l}|\mathbf{m})} \\ &= \mathbb{E}_{\mathbf{m}, \mathbf{l}} \log \frac{q(\mathbf{l}|\mathbf{m})}{p(\mathbf{l})} + \mathbb{E}_{\mathbf{m}, \mathbf{l}} \log \frac{p(\mathbf{m}, \mathbf{l})}{q(\mathbf{m}, \mathbf{l})} - \mathbb{E}_{\mathbf{m}} \log \frac{p(\mathbf{m})}{q(\mathbf{m})} \\ &\geq \mathbb{E}_{\mathbf{m}, \mathbf{l}} \left[ \log \frac{q(\mathbf{m}, \mathbf{l})}{p(\mathbf{m})P(\mathbf{l})} \right]. \end{aligned} \quad (18)$$

The inequality (18) holds since the KL divergence maintains non-negativity. The lower bound is tight when  $q(\mathbf{m}, \mathbf{l})$  converges to  $p(\mathbf{m}, \mathbf{l})$ . However,  $q(\mathbf{m}, \mathbf{l})$  has to satisfy the probability constraint axioms such as non-negativity, symmetry, and summary of all probability values equal to one. By [32],  $q(\mathbf{m}, \mathbf{l})$  is represented by an unconstrained function  $g(\gamma)$ , given as

$$q(\mathbf{m}, \mathbf{l}) = \frac{p(\mathbf{m})p(\mathbf{l})}{\mathbb{E}_{l_i \sim p(\mathbf{l})} \exp f_\theta(\mathbf{m}, l_i)} \exp g_\gamma(\mathbf{m}, \mathbf{l}). \quad (19)$$

Given a neural network  $AE(\mathbf{m}, \mathbf{l})$ , the Softmax activation function at the last layer is  $S(AE(\mathbf{m}, \mathbf{l})) : \mathbb{R}^M \rightarrow \mathbb{R}^M$  and defined as:

$$S(AE(\mathbf{m}, \mathbf{l})) = \frac{\exp AE(\mathbf{m}, \mathbf{l})}{\sum_{l_i=1}^M \exp n(M)_{l_i}}. \quad (20)$$

Then, the expected cross-entropy  $L_{CE}$  loss is given as

$$L_{CE} = -\mathbb{E}_{\mathbf{m}, \mathbf{l}} \left\{ AE(\mathbf{m}, \mathbf{l}) - \log \sum_{l_i=1}^M \exp AE(\mathbf{m}, \mathbf{l}) \right\} \quad (21)$$

where the expectation is taken over the joint distribution  $p(\mathbf{m}, \mathbf{l})$ . The following theorem presents the relationship between the estimated MI and the AE classifier.

**THEOREM 1.** *Let  $g_\gamma(\mathbf{m}, \mathbf{l}) = AE(\mathbf{m}, \mathbf{l})$ . The infimum of the expected cross-entropy loss with output of Softmax activation function  $S(AE(\mathbf{m}, \mathbf{l}))$  is equivalent to the MI between input and output variables  $\mathbf{m}, \mathbf{l}$ , respectively, up to constant  $\log M$  under uniform label distribution.*

*Proof.* Let  $g_\gamma(\mathbf{m}, \mathbf{l}) = AE(\mathbf{m}, \mathbf{l})$ , then the lower bound is

$$\mathbb{E}_{\mathbf{m}, \mathbf{l}} \log \frac{\exp AE(\mathbf{m}, \mathbf{l})}{\sum_{l_i=1}^M \exp AE(\mathbf{m}, \mathbf{l})_{l_i}}. \quad (22)$$

If the distribution of the label is uniform, we can rewrite

$$\begin{aligned} &\mathbb{E}_{\mathbf{m}, \mathbf{l}} \log \frac{\exp AE(\mathbf{m}, \mathbf{l})}{\frac{1}{M} \sum_{l_i=1}^M \exp AE(\mathbf{m}, \mathbf{l})_{l_i}} \\ &= \mathbb{E}_{\mathbf{m}, \mathbf{l}} \log \frac{\exp AE(\mathbf{m}, \mathbf{l})}{\sum_{l_i=1}^M \exp AE(\mathbf{m}, \mathbf{l})_{l_i}} + \log M \\ &= -S(AE(\mathbf{m}, \mathbf{l})) + \log M, \end{aligned} \quad (23)$$

which is equivalent to the negative expected cross-entropy loss up to constant  $\log M$ . Hence, the infimum of the expected

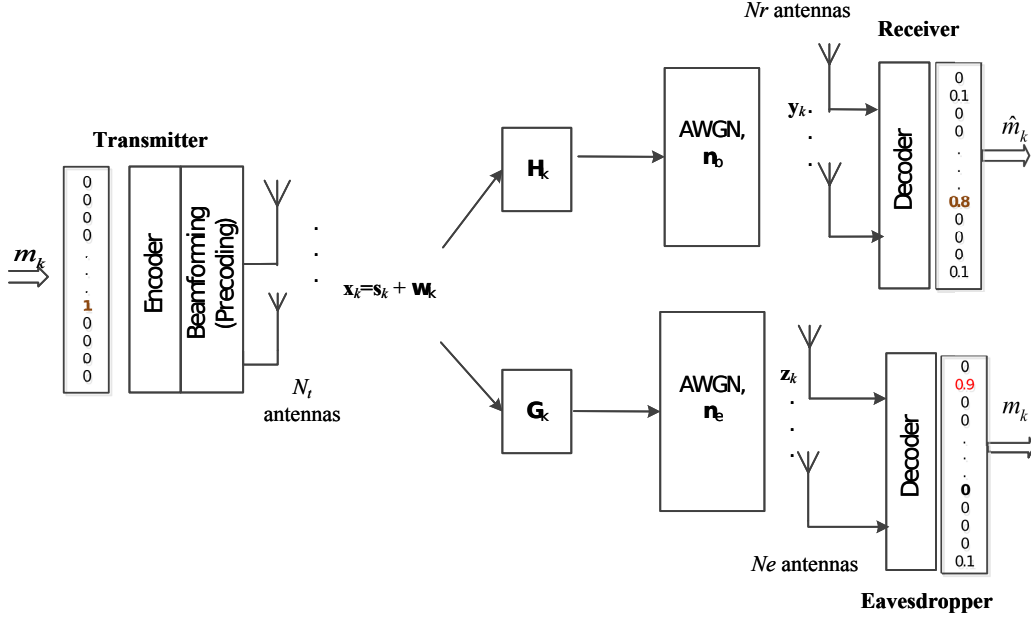


Fig. 3: AE-based MIMO FJ.

cross-entropy equals the MI between input and output variables.

Therefore, the secrecy optimization can be transformed into the cross-entropy optimization between the transmitted and received signals. Next, we construct a new cross-entropy loss function to optimize the MIMO-AE channel parameters.

### B. Security Loss Function

The term security loss function was first proposed in [22], which is a mixed loss cross-entropy function aiming to maximize the ML between the transmitted and received signals at the Rx and increase the cross-entropy between the transmitted and the received signals at the eavesdropper. However, this assumption may not be available in practical scenarios because eavesdroppers are passive and would never give feedback for the training process. In our work, we propose the following cross-entropy loss function:

$$L = (1 - \alpha)H(p_A(s_k), p_B(s_k)) + \alpha H(p_A(w_k), p_B(w_k)) \quad (24)$$

where  $p_A(s_k)$  and  $p_B(s_k)$  are the probability mass functions of the information signals, and  $p_A(w_k)$  and  $p_B(w_k)$  are the resulting probability mass functions of the FJ signals at the Tx and the Rx, respectively,  $H(\cdot)$  denotes the cross-entropy, and  $\alpha$  is a parameter for the security and communication rate trade-off. Hence, minimizing  $H(p_A(s_k), p_B(s_k))$  or maximizing the output probability of symbol  $s_{ik}$  will decrease the output probability of all other symbols at the Rx. In contrast, maximizing  $H(p_A(s_k), p_E(s_k))$  forces the system to reduce the output probability of the symbol  $s_{ik}$ , resulting in a higher probability on other symbols  $s_{jk}$ ,  $i \neq j$ . In other words, this scheme can minimize the MI  $I(FJ, B)$  and maximize  $I(A, B)$ . As discussed, the AE classification task with softmax and cross-entropy loss function is equivalent to the maximum MI between the input and output. Hence, minimizing the loss

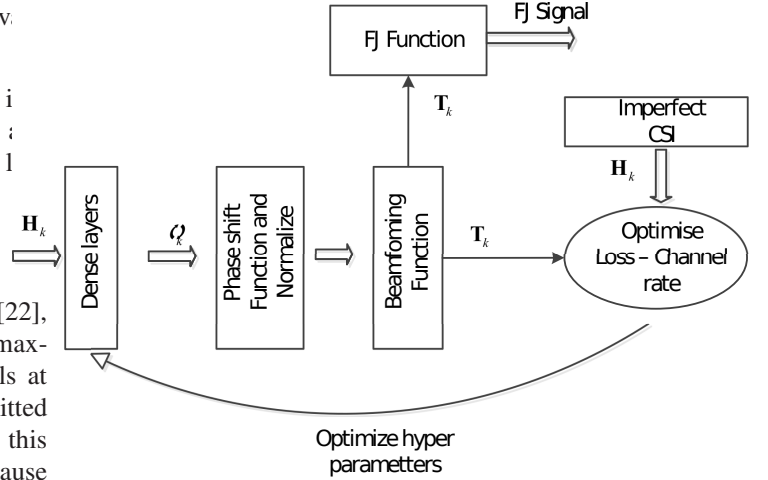


Fig. 4: The learning-based capacity driven FJ.

function (24) will reduce the effect of FJ on the Rx and maximize  $I(A, B)$ . By contrast, the eavesdropper channel will be degraded with a high probability since the eavesdropper does not have any information about the FJ signals.

### C. FJ Generation

To generate FJ signals, we propose a learning-based capacity-driven FJ (LCD-FJ) model, illustrated in Fig. 4. The LCD-FJ structure consists of an embedding layer that converts complex values of the inputs into real values, fully connected layers, and three Lambda functions. The first Lambda function is used to encode the input to the azimuth. The second Lambda function is used to design the precoding matrix  $\mathbf{T}_k$ , and the data rate is then calculated. The training process aims to optimize the precoding matrix  $\mathbf{T}_k$  by minimizing the loss function. As mentioned, the FJ signal is generated in the nullspace of

$\mathbf{T}_k$ , defined by the third Lambda function, so the FJ signal is as orthogonal as possible with the legitimate channel.

#### IV. MINE-BASED MIMO FJ

In the previous section, we proposed the AEFJ method for secure communication, where the secrecy was optimized based on the E2E learning process with ImCSI. In this section, we propose a MINE-based FJ method to deal with the scenarios when even the SCS is unavailable at the Tx.

##### A. MINE-based MIMO Communication

The MINE concept proposed in [23] estimates the MI between two random variables  $X$  and  $Y$  without knowing their distribution functions. The authors in [22] leveraged MINE for channel coding by estimating and maximizing the MI between the Tx and Rx symbols on the Gaussian single-input-single-output (SISO) communication channel. In this work, we introduce the MINE-based MIMO communication as illustrated in Fig. 5. The encoder and decoder resemble the AE-based communication.

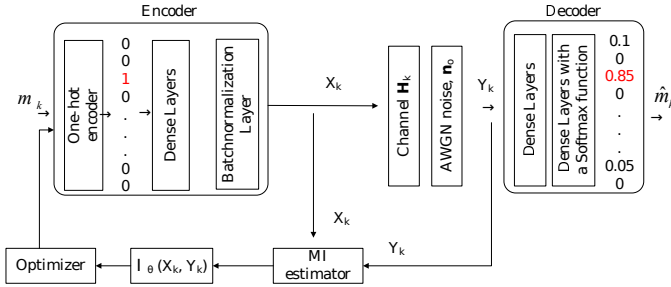


Fig. 5: The MINE-based MIMO channel.

The MI between the channel input and output samples will be estimated and maximized by optimizing the weights of the encoder. The MI between  $X$  and  $Y$  can be denoted as follows:

$$I(X, Y) = D_{KL}(p_{XY} \parallel p_X \otimes p_Y), \quad (25)$$

where  $D_{KL}$  is Kullback–Leibler divergence between the joint density  $p_{XY}$  and the product of the marginal densities  $p_X \otimes p_Y$ . The Donsker-Varadhan representation [23] can then be applied to represent the KL divergence as

$$D_{KL}(p \parallel q) = \sup_{F_{\Theta}: \Omega \rightarrow \mathbb{R}} \mathbb{E}_p f - \log \mathbb{E}_q e^f, \quad (26)$$

where the supremum is taken over all function classes  $f$  such that the expectation is finite. Assume  $T_{\theta}(X_n, Y_n) : X \times Y \rightarrow \mathbb{R}$  is a function in the class function  $f$ , with parameters  $\theta \in \Theta$  in the family function  $F_{\Theta}$ . The transmit and receive symbols in one channel instance are denoted by  $X_n$  and  $Y_n$ . When  $p = p_{XY}$  and  $q = p_X \otimes p_Y$  Then,  $D_{KL}(p \parallel q) = I(X, Y)$  mutual information  $I(X, Y)$  is given by

$$I(X, Y) \geq \sup_{T_{\theta} \in F_{\Theta}} \mathbb{E}_p T_{\theta}(X_n, Y_n) - \log \mathbb{E}_q e^{T_{\theta}(X_n, Y_n)}. \quad (27)$$

$I(X, Y)$  is estimated by its lower bound  $I_{\Theta}(X, Y)$  [23], known as the statistical MI between  $X$  and  $Y$  and is given by

$$I_{\Theta}(X, Y) = \sup_{\theta \in \Theta} \mathbb{E}_{p_{XY}} T_{\theta}(X_n, Y_n) - \log \mathbb{E}_{p_X \otimes p_Y} e^{T_{\theta}(X_n, Y_n)}. \quad (28)$$

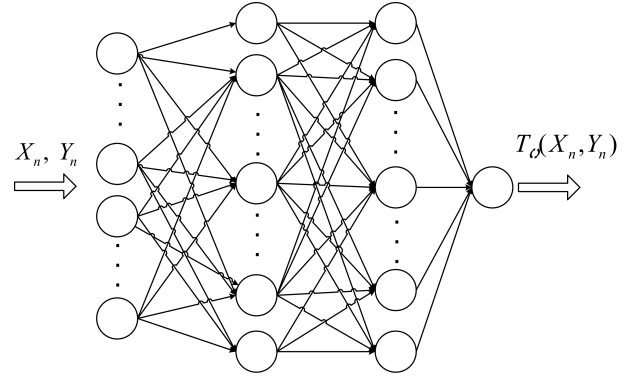


Fig. 6: MI estimator. The inputs are the samples of Tx and Rx signals at the Rx and eavesdropper. The output is the estimated MI on the legitimate and illegitimate channels.

The estimator  $T_{\theta}(X_n, Y_n)$  model contains two fully connected hidden layers with the ReLU activation function and an output node, which is depicted in Fig. 6. The inputs are the samples of the Tx signals that follow the joint density  $p_{XY}$  or  $p_{XZ}$ , and marginal densities  $p_X$ ,  $p_Y$  or  $p_Z$ , respectively. We then approximate the expectations by using the sample average method. The marginal  $p_X$  and  $p_Y$  can be derived by using the sampled average method, where the samples are shuffled from the joint distribution in the batch dimension [23]. The estimated statistical MI between the Tx and the Rx is then can be expressed as follows:

$$I_{\Theta}(X_n, Y_n) = \frac{1}{N} \sum_{i=1}^N T_{\theta}(\mathbf{x}_i^n, \mathbf{y}_i^n) - \log \frac{1}{N} \sum_{i=1}^N e^{T_{\theta}(\mathbf{x}_i^n, \bar{\mathbf{y}}_i^n)}, \quad (29)$$

where  $\mathbf{x}_i^n$  and  $\bar{\mathbf{y}}_i^n$  are the elements in the sets of samples  $X_n$  and  $Y_n$ , respectively. The optimization process is performed alternatively between the MINE network and the encoder with the weights  $\theta$  and  $\phi$ , respectively. This training process also optimizes the block error rate when the decoder is pre-trained separately from the encoder, making the training more flexible.

##### B. MINE-based MIMO FJ Scheme

The main advantage of MINE is that it can estimate and maximize the MI between two random variables without the need for joint probability distribution between them. The goal here is to maximize the MI between the Tx and the Rx,  $I(A, B)$ , while minimizing the MI between the Tx and the eavesdropper,  $I(A, E)$ . The MINE-based FJ is presented in Algorithm 1. We assume that the eavesdropper has the full knowledge of CSI. The receive symbol in channel instance  $n$  is denoted as  $Z_n$ . Following (29), the estimated MI between  $X_n$  and  $Z_n$  can be expressed as

$$I_{\Theta}(X_n, Z_n) = \frac{1}{N} \sum_{i=1}^N T_{\theta_2}(\mathbf{x}_i^n, \mathbf{z}_i^n) - \log \frac{1}{N} \sum_{i=1}^N e^{T_{\theta_2}(\mathbf{x}_i^n, \bar{\mathbf{z}}_i^n)}, \quad (30)$$

where  $\theta_2$  is the parameters of the neural estimator at the eavesdropper. The encoder and MI estimator structures, i.e.,  $I_{\Theta}$  network, remain unchanged as described in Section IV-A. The MINE-based FJ scheme will combine the MI estimator and

---

**Algorithm 1** MINE-based MIMO Friendly Jamming
 

---

- 1: At time  $k$ : Generate  $\mathbf{w}_k = \mathbf{Z}_k \mathbf{v}_k$ , orthogonal to  $\mathbf{H}_k^\dagger$
  - 2: Tx transmits  $\mathbf{x}_k = \mathbf{s}_k + \mathbf{w}_k$
  - 3: Rx receives  $\mathbf{y}_k$
  - 4: **for**  $i=1$  to Iteration **do**
  - 5:   Maximize estimated MI  $I_{AB}^{(i)}$
  - 6:   Save estimated  $I_{AB}^{(i)}$
  - 7:   Load  $I_{AB}^{(i)}$  as loss value to optimize encoder weights by performing gradient descent steps
  - 8:   Set  $i = i + 1$
  - 9:   **if**  $I_{AB}^{(i+1)} \leq I_{AB}^{(i)}$  **then**
  - 10:     break
  - 11:   **end if**
  - 12: **end for**
- 

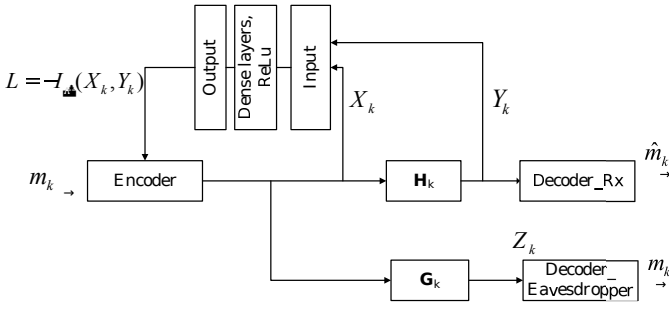


Fig. 7: MINE-based FJ.

encoder with the injected FJ signals, as illustrated in Fig. 7. The model takes the input as the sampled signals  $X_n$  and  $Y_n$  to estimate  $I_\Theta(A, B)$ . The value of  $I_\Theta(A, B)$  is fed back to the encoder for adjusting the hyperparameters, weights, and biases. The same process is repeated until  $I_\Theta(A, B)$  is maximized.

To fulfill both security and transmission reliability objectives, we introduce the following novel security loss function:

$$L_{\text{MINE}} = \beta I_\Theta(X_n, Y_n) + (1 - \beta) I_\Theta(X_n, Z_n), \quad (31)$$

where  $\beta$  is a coefficient that controls the trade-off between communication rate and security. Then, the loss function can be further written as follows:

$$L_{\text{MINE}} = \frac{\beta}{N} \sum_{i=1}^N T_\theta(\mathbf{x}_i^n, \mathbf{y}_i^n) - \beta \log \frac{1}{N} \sum_{i=1}^N e^{T_\theta(\mathbf{x}_i^n, \bar{\mathbf{y}}_i^n)} - \frac{1 - \beta}{N} \sum_{i=1}^N T_\theta(\mathbf{x}_i^n, \bar{\mathbf{z}}_i^n) + (1 - \beta) \log \frac{1}{N} \sum_{i=1}^N e^{T_\theta(\mathbf{x}_i^n, \bar{\mathbf{z}}_i^n)}. \quad (32)$$

Furthermore, we consider the worst case when the noise power at the eavesdropper  $\sigma_e^2 = 0$  [9]. Then, the covariance of noise at Eve in (3) becomes  $\mathbf{K}'_k = (\mathbf{G}_k \mathbf{Z}_k \mathbf{Z}_k^\dagger \mathbf{G}_k^\dagger) \sigma_v^2$ . To simplify the notation, all occurrences of  $R_k^S$  will be understood

as representing GSC from this point forward. Then, the guaranteed secrecy rate (GSC) is given by

$$R_k^S = I_\Theta(X_n, Y_n) - R_{AE\max} = I_\Theta(X_n, Y_n) - \log \frac{\det(\mathbf{K}'_k + \mathbf{G}_k^\dagger \mathbf{Q}_s \mathbf{G}_k)}{\det \mathbf{K}'_k}. \quad (33)$$

That optimization problem can be resolved by performing SVD on  $\mathbf{H}_k$  and the second-order perturbation analysis [17]. However, this method requires exponential complexity when the number of antennas increases. Thus, we leverage the non-convex optimization capability provided by deep neural networks and then directly solve the problem with sufficient training data by considering the CSI error as an input for the training process.

## V. SIMULATION RESULTS AND DISCUSSION

### A. Simulation Setups and Parameters

In this section, we use the Montecarlo method to evaluate the effectiveness of the proposed approaches. The secrecy rate is averaged over  $10^6$  iterations. The channels  $\mathbf{H}_k$  and  $\mathbf{G}_k$  are generated as complex Gaussian matrix [30], where  $h_{i,j}$  and  $g_{i,j}$  are assumed to be i.i.d. Gaussian with  $\mathbb{E}|h_{i,j}|^2 = \mathbb{E}|g_{i,j}|^2 = 1$ . The real and imaginary parts of the entries in the channel matrices  $\mathbf{H}_k$  and  $\mathbf{G}_k$  are standard Gaussian i.i.d.. We generate a complex-valued channel matrix where the real and imaginary parts are normally distributed. This results in a Rayleigh-distributed channel matrix magnitude commonly used to model fading in wireless communication channels. The phase of the channel follows a uniform distribution from 0 to  $2\pi$ . The total power  $P_{\max}$  is normalized by the power of AWGN noise  $\sigma_n^2 = \sigma_e^2 = 1$ . The SNR values in the training are set to vary from 10 dB to 25 dB, guaranteeing the generality of the trained model. For analysis, the eavesdropper is assumed to have the same neural architecture decoder as the Rx, as in Fig. 3. The AE at the Tx-Rx channel inducing FJ and the network at the eavesdropper are trained simultaneously as a one-input-two-output network with the loss function in (24).

To see the advantages of the proposed method, we compare our method with two baselines proposed in [9] and [17]. The former first uses multiplexing as the precoding technique and then adopts executive search to optimize the average secrecy rate  $R_{kex}^S$ . Differently, the latter is based on the perturbation/error second-order analysis, called ‘‘So’’, to optimize the average secrecy rate  $R_{kSo}^S$ . Further, we use the state-of-the-art DL library Tensor Flow with Adam Optimizer for training. The input and output layers have 16 neurons, representing a symbol of 4 bits. The channel layer includes  $N_t$  neuron width representing the number of transmit antennas. The network architecture and its parameters are summarized in Table I.

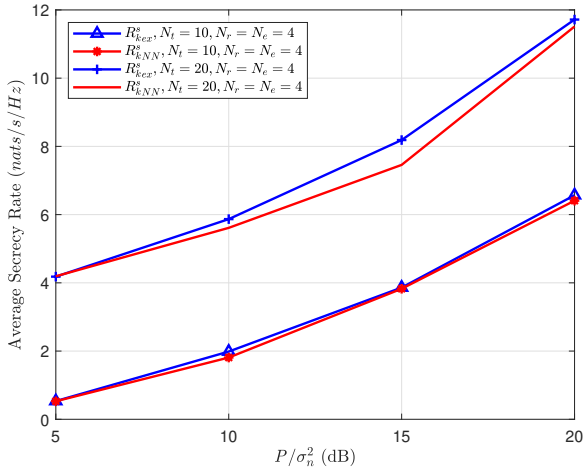
### B. Experimental Results

We first implement the AE-based FJ model in the case of perfect CSI and compare its performance with that of the exhaustive search method in [9], as shown in Fig. 8. In the AEFJ method, the channel matrix is considered an extra input parameter at the encoder and decoder in the AEFJ model. The



TABLE I: Architecture and Parameters of LCD-FJ Model

Layer (type), number of nodes	Output shape	# parameters
imperfect_CSI (InputLayer)	[(None, 1, 2, 64)]	0
batch_normalization_24 (BatchNormalization)	(None, 1, 2, 64)	256
flatten_8 (Flatten)	(None, 128)	0
batch_normalization_25 (BatchNormalization)	(None, 128)	512
dense_24 (Dense)	(None, 256)	33,024
batch_normalization_26 (BatchNormalization)	(None, 256)	1,024
dense_25 (Dense)	(None, 128)	32,896
dense_26 (Dense)	(None, 64)	8,256
perfect_CSI (InputLayer)	[(None, 64)]	0
lambda_16 (Lambda)	(None, 64)	0
SNR_input (InputLayer)	[(None, 1)]	0
lambda_17 (Lambda)	(None, 1)	0

Fig. 8: Average secrecy rate versus  $P_{\max}/\sigma_n^2$  under ImCSI.

parameter  $\alpha$  was chosen as 0.5 to make the balance between transmission and capacity. We consider two different values of the number of antennas at the Tx;  $N_t = 10, 20$ . As can be seen, the average secrecy rate of the proposed AEFJ method is close to that of the optimal scheme, i.e., the exhaustive search [9]), when the number of antennas at the Tx is small,  $N_t = 4$ , confirming the effectiveness of the proposed AEFJ scheme. This can be explained by the capability of the AE to learn the features of channel distribution with sufficient data and perfect CSI.

Regarding BLER, Fig. 9 shows the BLER of the proposed method at the Rx and the eavesdropper. By assuming that the eavesdropper and the Rx have the same model, we can see that the BLER at the eavesdropper's decoder is much higher than the Rx's. Although the BLER of the proposed method is higher than that of the ML-based method, the former provides much less computational complexity than the latter.

Regarding ImCSI, our target is to compare the average secrecy rate achieved by our method with the work [17], where full CSI is unavailable at the Tx. The parameter  $\sigma_e = -20$  dB or 0.1 represents the level of perturbation or channel estimation error. The security communication model is illustrated in Table II. As shown in Fig. 10, the proposed AEFJ scheme offered a better average secrecy rate than So

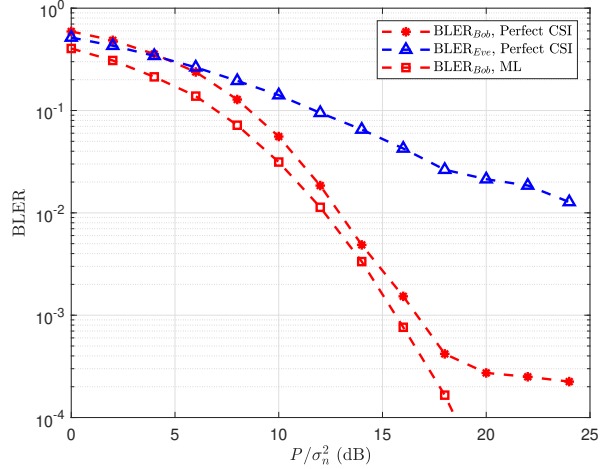
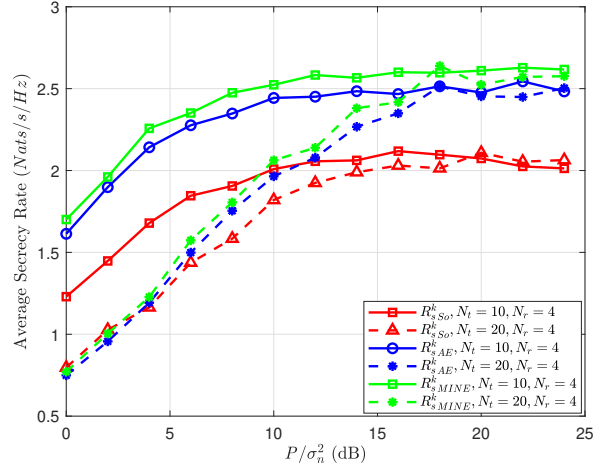
Fig. 9: BLER at Rx and eavesdropper with FJ;  $\mathbf{H}_k$  perfectly known.Fig. 10: Average secrecy rate versus  $P/\sigma_n^2$  (dB).

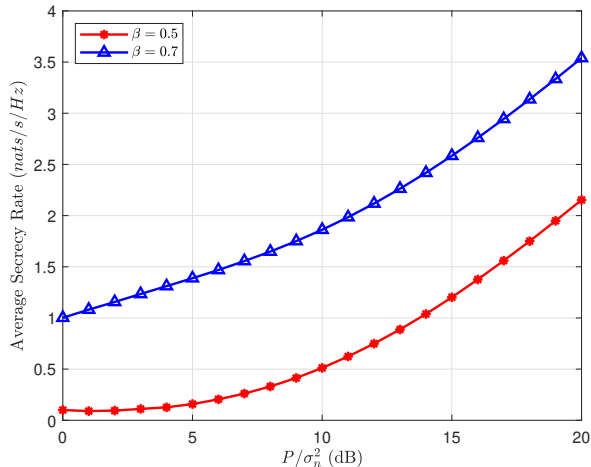
TABLE II: Architecture and Parameters of AEFJ with SCS

Encoder	Encode a message $m_k$ to $s_k$
LCD FJ	$w_k$ orthogonal to $s_k$
Power constraints/norm	Normalize average power
Channel	Generate random complex channel $H_k$
Lambda	Matrix multiplication $x_k$ with $H_k$
Dense	Simulate Tx-Rx channel, estimating mapping function $Q(x_k, \hat{H}_k)$
Softmax function	Calculate loss to optimize tMI

based-method [17]. We note that the secrecy rate increased linearly at the low SNR region but tended to be saturated at high normalized transmit power, i.e., from 10 dB to 25 dB. In addition, the higher secrecy rate can be seen in the MINE-based method compared to AEFJ [33]. The reason is the former optimizes the MI directly while the latter depends on the cross entropy loss. Moreover, the higher the number of transmit antennas, the higher the secrecy rate for both schemes. This stems from the fact that the proposed AE architecture can effectively perform denoising and capturing

TABLE III: Description of function layers in AEFJ with ImCSI

Input	Concatenate $x_k$ and $\hat{H}_k$ , converted to real domain from complex domain
Power constraints/norm	Normalize average power
Channel	Generate imperfect complex channel $\hat{H}_k$
Lambda	Matrix multiplication $x_k$ with $\hat{H}_k$
Hidden	Simulate Tx-Rx channel, estimating mapping function: $Q(x_k, \hat{H}_k)$
Output Layer	$\hat{x}_k$ , and the activation function is soft-max for a reconstruction problem
Optimizer	Adam optimizer
Loss Function	Equation (18)

Fig. 11: Average secrecy rate with different values of  $\beta$ .

features of the channel with sufficient data. The MINE security loss function (32) is used to evaluate the performance of the security approach. The network architecture of the MINE-FJ scheme is shown in Table III.

Fig. 11 illustrates the secrecy rate with two different values of  $\beta$ , where the number of transmit antennas is  $N_t = 3$ , each with 400 iterations and the batch size of 20,000. We observe that the higher the value of  $\beta$ , the higher the secrecy rate was obtained. This shows the trade-off between the communication and secrecy rates due to the influence of the FJ signal. Fig. 12 shows BLER at both the Rx and the eavesdropper in a range of SNR values before and after a secure communication was applied by AEFJ. The black curves represent BLER at Rx when using MINE-based FJ with and without FJ. The red curves represent BLER at Rx when using AE-based FJ with and without FJ, whereas the blue curve illustrates the BLER at the eavesdropper. We notice two important points. Firstly, the BLER at Rx increased, with the gap of 3dB at  $10^{-4}$  of BLER. It can be explained that a portion of power is allocated for jamming. Secondly, there was a significant increase in the BLER at the eavesdropper using AEFJ. The higher BLER at the eavesdropper is because of the effect of FJ signals on the eavesdropper channel, which makes the information signals undecodable at the eavesdropper.

In Fig. 13, the convergence of MINE-FJ is provided with different SNR levels using the security model in Fig. 7. It can be seen that the MINE approach quickly converged to

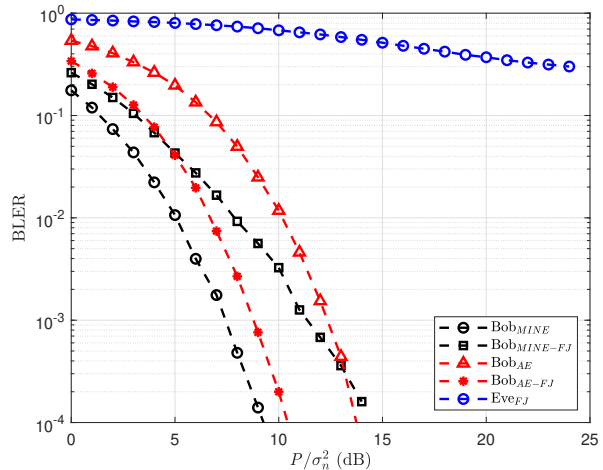
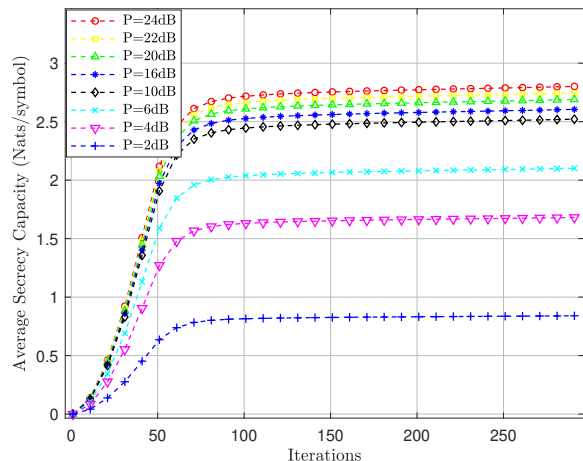


Fig. 12: BLER at Rx and eavesdropper with AEFJ and MINE-FJ.

Fig. 13: Secrecy rate vs. number of iterations;  $N_t = 10$ ,  $N_r = 4$  and  $N_e = 4$ .

a stationary point after about 100 iterations. In addition, the secrecy rate improved dramatically when the SNR increased but tended to saturate for a sufficiently high SNR. This saturation can be explained as when the distribution of the transmit is close to receiving samples.

The relationship between the average secrecy rate and the number of transmit antennas is provided in Fig. 14. It shows that the average secrecy rate increased rapidly with the number of antennas  $N_t$ . This is attributed to the fact that the higher the number of transmit antennas at the Tx, the more the degree of freedom can be added to the system to transmit the desired signal and design the FJ signal more effectively. In Fig. 15, we show a trade-off between the secrecy rate and BLER with and without using FJ. As expected, the higher the BLER, the lower the average secrecy rate is obtained.

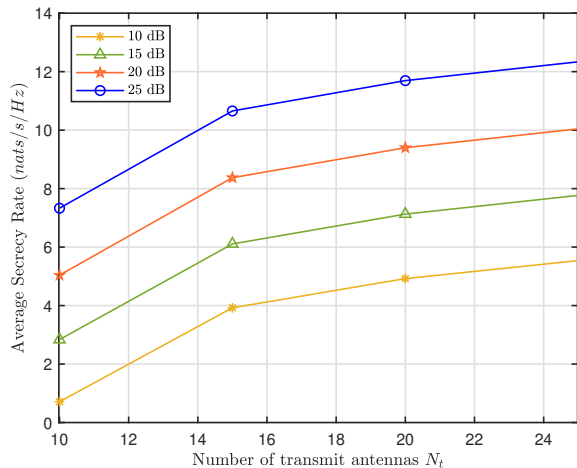


Fig. 14: Secrecy rates vs.  $N_t$ .

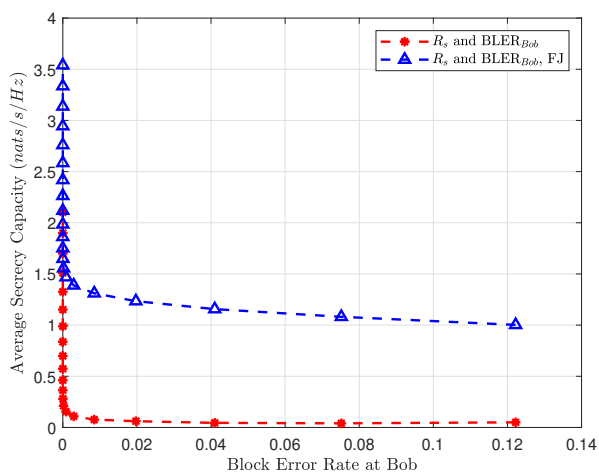


Fig. 15: Average secrecy rate and BLER at Rx;  $N_t = 10$ ,  $N_r = 4$  and  $N_e = 4$ .

### C. Complexity

This subsection compares the computational complexity as the number of floating-point operations (FLOPs) between AEFJ and the conventional methods. Herein, we only counted the complexity in the deployment stage since the training stage can be seen as offline. The number of FLOPs of a dense layer is referred to in the work in [34], which is equal to  $(2N_{Input} - 1)N_{Output}$ , where  $N_{Input}$  and  $N_{Output}$  are the input and output dimensions, respectively. For example, when  $N_t = 20$  and the transmit symbol is encoded into a one-hot vector and considering the architecture of our model in Table IV, the FLOPs is 6,144. For the exhausting search and “So” method mentioned previously, the asymptotic computational complexity is in the order of  $O(N_t^3)$  as they perform SVD and matrix inversion.

## VI. CONCLUSION

In this paper, we have introduced a novel DL-based FJ approach to deal with the eavesdropping issues in MIMO-

TABLE IV: Parameters and FLOP of AEFJ.

Name of Layers	Input and Output Dimensions	FLOPs
Input Layer	16; 64	2,048
Dense Layer 2	64; 8	1,024
Dense Layer 3	8; 64	1,024
Output layer	64; 16	2,048

based systems. First, we have proposed the AEFJ scheme by leveraging the E2E learning at both the Tx and the Rx, which has shown to achieve both communication secrecy and reliability compared to the conventional methods. In addition, we have leveraged MINE to design a robust security scheme without SCSI at Tx. Simulation results have showed the comparable security performance of MINE to AEFJ under the cross-entropy security loss function. Further, the secrecy rate was optimized independently at the Tx and the Rx using the MI neural estimator. Thus, the MINE-based FJ is promising for applications that require fast deployment and lightweight but effective security methods. This can be seen as a lightweight solution since the training process is not heavily based on channel estimation and capturing the symbol but does not require the demodulation and decoding steps.

## REFERENCES

- [1] A. Mukherjee, S. A. A. Fakoorian, J. Huang, and A. L. Swindlehurst, “Principles of physical layer security in multiuser wireless networks: A survey,” *IEEE Commun. Surv. Tutor.*, vol. 16, no. 3, pp. 1550–1573, 2014.
- [2] Y. Zhang, Y. Shen, H. Wang, J. Yong, and X. Jiang, “On secure wireless communications for iot under eavesdropper collusion,” *IEEE Transactions on Automation Science and Engineering*, vol. 13, no. 3, pp. 1281–1293, 2015.
- [3] N. H. Chu, N. Van Huynh, D. N. Nguyen, D. T. Hoang, S. Gong, T. Shu, E. Dutkiewicz, and K. T. Phan, “Countering eavesdroppers with meta-learning-based cooperative ambient backscatter communications,” *arXiv preprint arXiv:2308.02242*, 2023.
- [4] D. J. Bernstein and T. Lange, “Post-quantum cryptography,” *Nature*, vol. 549, no. 7671, pp. 188–194, 2017.
- [5] M. Bloch, J. Barros, M. R. Rodrigues, and S. W. McLaughlin, “Wireless information-theoretic security,” *IEEE Trans. Inf. Theory*, vol. 54, no. 6, pp. 2515–2534, 2008.
- [6] C. E. Shannon, “Communication theory of secrecy systems,” *The Bell System Technical Journal*, vol. 28, no. 4, pp. 656–715, 1949.
- [7] A. D. Wyner, “The wire-tap channel,” *Bell System Technical Journal*, vol. 54, no. 8, pp. 1355–1387, 1975.
- [8] J. M. Hamamreh, H. M. Furqan, and H. Arslan, “Classifications and applications of physical layer security techniques for confidentiality: A comprehensive survey,” *IEEE Commun. Surv. Tutor.*, vol. 21, no. 2, pp. 1773–1828, 2018.
- [9] S. Goel and R. Negi, “Guaranteeing secrecy using artificial noise,” *IEEE Trans. Wireless Commun.*, vol. 7, no. 6, pp. 2180–2189, 2008.
- [10] B. Akgun, O. O. Koyluoglu, and M. Krunz, “Exploiting full-duplex receivers for achieving secret communications in multiuser MISO networks,” *IEEE Trans. Commun.*, vol. 65, no. 2, pp. 956–968, 2016.
- [11] P. Siyari, M. Krunz, and D. N. Nguyen, “Friendly jamming in a mimo wiretap interference network: A nonconvex game approach,” *J. Sel. Areas Commun.*, vol. 35, no. 3, pp. 601–614, 2017.
- [12] J. Choi, “A robust beamforming approach to guarantee instantaneous secrecy rate,” *IEEE Trans. Wireless Commun.*, vol. 15, no. 2, pp. 1076–1085, 2015.
- [13] D. N. Nguyen and M. Krunz, “Spectrum management and power allocation in mimo cognitive networks,” in *2012 Proceedings IEEE INFOCOM*, 2012, pp. 2023–2031.
- [14] —, “Price-based joint beamforming and spectrum management in multi-antenna cognitive radio networks,” *IEEE Journal on Selected Areas in Communications*, vol. 30, no. 11, pp. 2295–2305, 2012.

- [15] T. X. Vu, S. Chatzinotas, V.-D. Nguyen, D. T. Hoang, D. N. Nguyen, M. D. Renzo, and B. Ottersten, "Machine learning-enabled joint antenna selection and precoding design: From offline complexity to online performance," *IEEE Transactions on Wireless Communications*, vol. 20, no. 6, pp. 3710–3722, 2021.
- [16] A. Mukherjee, "Physical-layer security in the internet of things: Sensing and communication confidentiality under resource constraints," *Proceedings of the IEEE*, vol. 103, no. 10, pp. 1747–1761, 2015.
- [17] A. Mukherjee and A. L. Swindlehurst, "Robust beamforming for security in mimo wiretap channels with imperfect csi," *IEEE Trans. Signal Process.*, vol. 59, no. 1, pp. 351–361, 2010.
- [18] M. Pei, J. Wei, K.-K. Wong, and X. Wang, "Masked beamforming for multiuser mimo wiretap channels with imperfect csi," *IEEE Trans. Wireless Commun.*, vol. 11, no. 2, pp. 544–549, 2012.
- [19] J. B. Perazzone, P. L. Yu, B. M. Sadler, and R. S. Blum, "Artificial noise-aided mimo physical layer authentication with imperfect csi," *IEEE Transactions on Information Forensics and Security*, vol. 16, pp. 2173–2185, 2021.
- [20] T. Erpek, T. J. O'Shea, and T. C. Clancy, "Learning a physical layer scheme for the mimo interference channel," in *2018 IEEE International Conference on Communications (ICC)*. IEEE, 2018, pp. 1–5.
- [21] T. J. O'Shea, T. Erpek, and T. C. Clancy, "Deep learning based MIMO communications," *arXiv preprint arXiv:1707.07980*, 2017.
- [22] R. Fritschek, R. F. Schaefer, and G. Wunder, "Deep learning for the gaussian wiretap channel," in *ICC 2019-2019 IEEE International Conference on Communications (ICC)*. IEEE, 2019, pp. 1–6.
- [23] M. I. Belghazi, A. Baratin, S. Rajeshwar, S. Ozair, Y. Bengio, A. Courville, and D. Hjelm, "Mutual information neural estimation," in *Proceedings of the 35th International Conference on Machine Learning*, ser. Proceedings of Machine Learning Research, J. Dy and A. Krause, Eds., vol. 80. PMLR, 10–15 Jul 2018, pp. 531–540. [Online]. Available: <https://proceedings.mlr.press/v80/belghazi18a.html>
- [24] N. A. Letizia and A. M. Tonello, "Capacity-driven autoencoders for communications," *IEEE Open Journal of the Communications Society*, vol. 2, pp. 1366–1378, 2021.
- [25] T. Lin and Y. Zhu, "Beamforming design for large-scale antenna arrays using deep learning," *IEEE Wireless Communications Letters*, vol. 9, no. 1, pp. 103–107, 2019.
- [26] R. Fritschek, R. F. Schaefer, and G. Wunder, "Deep learning for channel coding via neural mutual information estimation," *arXiv preprint arXiv:1903.02865*, 2019.
- [27] C. Wang, E. K. S. Au, R. D. Murch, W. H. Mow, R. S. Cheng, and V. Lau, "On the performance of the mimo zero-forcing receiver in the presence of channel estimation error," *IEEE Trans. Wireless Commun.*, vol. 6, no. 3, pp. 805–810, 2007.
- [28] T. O'Shea and J. Hoydis, "An introduction to deep learning for the physical layer," *IEEE Trans. Cogn. Commun. Netw.*, vol. 3, no. 4, pp. 563–575, 2017.
- [29] Y. Bengio, I. Goodfellow, and A. Courville, *Deep learning*. MIT Proess, 2017, vol. 1.
- [30] E. Telatar, "Capacity of multi-antenna gaussian channels," *Eur. Trans. Telecommun.*, vol. 10, no. 6, pp. 585–595, 1999.
- [31] D. B. F. Agakov, "The im algorithm: a variational approach to information maximization," 2004.
- [32] D. McAllester and K. Stratos, "Formal limitations on the measurement of mutual information," in *Procee. of the Twenty Third International Conference on Artificial Intelligence and Statistics*, ser. Proceedings of Machine Learning Research, S. Chiappa and R. Calandra, Eds., vol. 108. PMLR, 26–28 Aug 2020, pp. 875–884.
- [33] F. Mirkarimi, S. Rini, and N. Farsad, "Benchmarking neural capacity estimation: Viability and reliability," *IEEE Trans Commun.*, vol. 71, no. 5, pp. 2654–2669, 2023.
- [34] A. Mohammad, C. Masouros, and Y. Andreopoulos, "Complexity-scalable neural-network-based mimo detection with learnable weight scaling," *IEEE Trans Commun.*, vol. 68, no. 10, pp. 6101–6113, 2020.